Nat. Hazards Earth Syst. Sci., 19, 629–653, 2019
https://doi.org/10.5194/nhess-19-629-2019

Natural Hazards and Earth System Sciences
Open Access
EGU

Application of the Levenburg–Marquardt back propagation neural network approach for landslide risk assessments

Junnan Xiong[1,3], Ming Sun[2], Hao Zhang[1], Weiming Cheng[3], Yinghui Yang[1], Mingyuan Sun[1], Yifan Cao[1], and Jiyan Wang[1]

[1]School of Civil Engineering and Architecture, Southwest Petroleum University, Chengdu, 610500, P.R. China
[2]The First Surveying and Mapping Engineering Institute of Sichuan Province, Chengdu, 610100, P.R. China
[3]State Key Laboratory of Resources and Environmental Information System, Institute of Geographic Science and Natural Resources Research, Chinese Academy of Sciences, Beijing, 100101, P.R. China

Correspondence: Junnan Xiong (neu_xjn@163.com) and Hao Zhang (zhanghao412658@163.com)

Received: 28 November 2018 – Discussion started: 6 December 2018
Revised: 25 February 2019 – Accepted: 27 February 2019 – Published: 25 March 2019

Abstract. Landslide disasters are one of the main risks involved with the operation of long-distance oil and gas pipelines. Because previously established disaster risk models are too subjective, this paper presents a quantitative model for regional risk assessment through an analysis of the patterns of historical landslide disasters along oil and gas pipelines. Using the Guangyuan section of the Lanzhou–Chengdu–Chongqing (LCC) long-distance multiproduct oil pipeline (82 km) in China as a case study, we successively carried out two independent assessments: a susceptibility assessment and a vulnerability assessment. We used an entropy weight method to establish a system for the vulnerability assessment, whereas a Levenberg–Marquardt back propagation (LM-BP) neural network model was used to conduct the susceptibility assessment. The risk assessment was carried out on the basis of two assessments. The first, the system of the vulnerability assessment, considered the pipeline position and the angle between the pipe and the landslide (pipeline laying environmental factors). We also used an interpolation theory to generate the standard sample matrix of the LM-BP neural network. Accordingly, a landslide susceptibility risk zoning map was obtained based on susceptibility and vulnerability assessment. The results show that about 70 % of the slopes were in high-susceptibility areas with a comparatively high landslide possibility and that the southern section of the oil pipeline in the study area was in danger. These results can be used as a guide for preventing and reducing regional hazards, establishing safe routes for both existing and new pipelines, and safely operating pipelines in the Guangyuan area and other segments of the LCC oil pipeline.

1 Introduction

By the year 2020, the total length of long-distance oil and gas pipelines is expected to exceed 160 000 km in China. This represents a major upsurge in the length of multinational long-distance oil and gas pipelines (Huo et al., 2016). The rapid development of pipelines is associated with significant geological hazards, especially landslides, which increasingly threaten the safe operation of pipelines (Wang et al., 2012; Yun and Kang, 2014; Zheng et al., 2012). Landslide disasters cause great harm to infrastructure and human life. Moreover, the wide impact area of landslides restricts the economic development of landslide-prone areas (Ding et al., 2016; Hong et al., 2015). A devastating landslide can lead to casualties, property loss, environmental damage, and long-term service disruptions caused by massive oil and gas leakages (G. Li et al., 2016; Zheng et al., 2012). Generally, pipeline failure or destruction caused by landslides is much more deleterious than the landslides themselves, which makes it important to research the risk assessment of geological landslide hazards in pipeline areas (Inaudi and Glisic, 2006; Mansour et al., 2011).

Natural disaster risk is comprised of a combination of natural and social attributes (Atta-Ur-Rahman and Shaw, 2015). The United Nations Department of Humanitarian Af-

fairs defines natural disaster risk as a product of susceptibility and vulnerability (Rafiq and Blaschke, 2012; Sari et al., 2017). In recent years, progress in geographic information systems (GIS) and remote sensing (RS) technologies have greatly enhanced our ability to evaluate the potential risks that landslides pose to pipelines (Akgun et al., 2012; Li and Gao, 2015; Sari et al., 2017). The disaster risk assessment model has been widely recognized and applied by experts and scholars all over the world. Landslide risk assessment can take the form of a qualitative (Wu et al., 1996), quantitative (Ho et al., 2000) or semiquantitative assessment (Liu et al., 2015) according to actual demand. Quantitative methods and models that have been proposed for the assessment can be divided into methods of statistical analysis (Sari et al., 2017), mathematical models (Akgun et al., 2012) and machine learning (He and Fu, 2009). However, most of these methods are subjective, such as expert evaluations, analytical hierarchy processes, logistic regressions and fuzzy integration methods, which could affect the accuracy and reasonableness of the evaluation (Fall et al., 2006; Sarkar and Gupta, 2005). This shortcoming can be overcome through the artificial neural network, especially the mature back propagation (BP) neural network that is widely used in function approximation and pattern recognition (Ke and Li, 2014a; Li et al., 2013; Su and Deng, 2003). The evaluation indicator system generally includes disaster characteristics, disaster prevention and pipeline attributes (Li, 2008, 2010). The fault tree analysis, fuzzy comprehensive evaluation and the grey theory are used to evaluate the failure probability of the system through indicator weight and scoring (Shi, 2011; Ye et al., 2013). In previous studies, pipeline vulnerability evaluation indicators only considered the pipeline itself, and the relationship between the pipeline and environment was rarely examined (Feng et al., 2014; Li, 2008; Liu et al., 2015). In this paper, the interaction between landslide hazards and the pipeline itself was considered, which improved the quantitative degree of the evaluation.

Based on the theory of the Levenberg–Marquardt back propagation (LM-BP) neural network, a standard sample matrix was developed using interpolation theory, after an analysis of the distribution characteristics of landslides that occurred in the study area was performed and a regional landslide susceptibility assessment was completed. Considering the interaction between landslide disasters and the pipeline itself, a pipeline vulnerability evaluation in the landslide area was realized using the entropy weight method. This paper establishes a risk assessment model and methods for assessing landslide geological susceptibility of oil pipelines by comprehensively utilizing GIS and RS technology, which together improves the quantitative degree of the assessment.

2 Study area

The study area was Guangyuan City in Sichuan province, which was further narrowed to the area from 105°15′ to 106°04′ E and 32°03′ to 32°45′ N, straddling 19 townships in five counties from south to north (Fig. 1). The Lanzhou–Chengdu–Chongqing (LCC) multiproduct oil pipeline is China's first long-distance pipeline. It begins in Lanzhou City and runs through Shanxi and Sichuan provinces (Hao and Liu, 2008). Our study area covered sloped areas of this range, with 5 km on both sides of the Guangyuan section (82 km) of the oil pipeline. The pipeline within the K558–K642 pipes may be affected by the slope areas. The Guangyuan section, located in northern Sichuan, is a transitional zone from the basin area to the mountain area. It features terrain of moderate and low mountains, crisscrossed networks of ravines and a strong fluvial incision. Altitudes in this area range from 328 to 1505 m. The study area has a subtropical monsoon climate with four distinctive seasons and annual precipitation measuring about 900 to 1000 mm. Moreover, two large unstable faults (the central fault of the Longmen Mountains and Longmen Mountains' Piedmont fault zone) make the area geologically unstable and prone to frequent geological hazards (Li et al., 2012). Guangyuan, through which the pipeline passes, has a high incidence of landslides, which have happened 300 times in the Lizhou and Chaotian districts (Zhang et al., 2011). In this area, landslide geological hazards seriously threaten the safe operation of the LCC oil pipeline.

3 Data sources

Landslide susceptibility assessment, pipeline vulnerability assessment and geological hazard risk assessment of the landslide pipeline were made successively. Digital elevation model (DEM) data with 30 m accuracy were sourced from the Geospatial Data Cloud (http://www.gscloud.cn/, last access: January 2017. Precipitation data were downloaded from the dataset of annual surface observation values in China between the years 1981 and 2010, as published by the China Meteorological Administration (http://data.cma.cn/, last access: January 2017). These data were collected from 18 meteorological observatories near and within the study area and interpolated using the kriging method (at a resolution of 30 m × 30 m). Geological maps and landslide data (historical landslides) in the study area were obtained from Sichuan province's geological environmental monitoring station. RS images (GF-1, multispectral 8 m, resolution 2 m) were provided by the Sichuan Remote Sensing Center.

The location of the middle line of the pipeline was detected through the direct connection method (i.e., the transmitter's output line was directly connected to the metal pipeline) using an RD8000 underground pipeline detector. Pipeline midline coordinates were measured using total network real-time

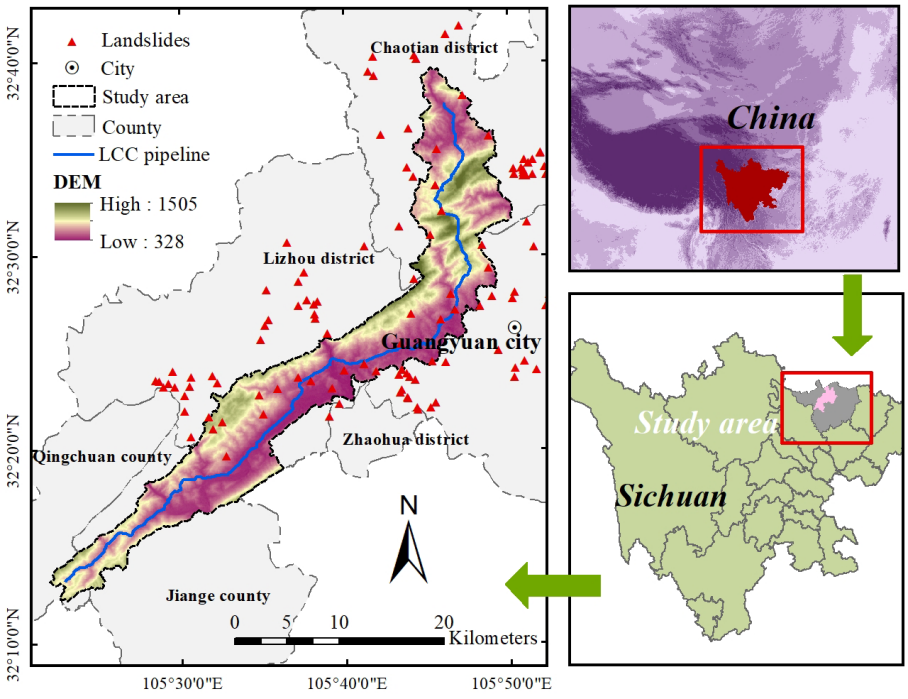

Figure 1. Landslide location map of the study area.

kinematic technology, and, simultaneously, the coordinates of the pipe ancillary facilities (including detective poles, mileage pegs and milestones) were acquired. Mileage data obtained through inner pipeline detection were derived from the China Petroleum Pipeline Company.

4 Methods

4.1 Assessment unit

Division precision and the scale of the slope unit (i.e., the basic element for a regional landslide susceptibility assessment) were in keeping with the results of the evaluation (Qiu et al., 2015). A total of 315 slope units were divided using hydrologic analysis in ArcGIS (v. 10.4) (Fig. 2a). The irrational unit (a slope unit with an inaccurate boundary) was artificially identified and modified by comparing GF-1 satellite remote sensing images. Boundary correction, fragment combination and fissure filling were used for modification.

This vulnerability study focuses on assessing the vulnerability of transport pipelines to landslides. Considering both previous research and the particulars of the research object, we used a comprehensive segmentation method based on GIS to divide the pipelines in our study. A total of 180 pipes were divided in the study area, of which the longest was about 1.7 km, and the shortest was only about 10 m (Fig. 2b).

4.2 Assessment indicators

Based on selection principles of the indicator system and the formation mechanism of landslide geological hazards, as few indicators as possible were selected to reflect the degree of danger posed by the landslide as accurately as possible (Avalon Cullen et al., 2016; Jaiswal et al., 2010; Ray et al., 2007). The internal factors in these indicators included topography, geological structure, stratigraphic lithology and surface coverage. Similarly, the external factors included mean annual precipitation (MAP) and the coefficient of the variation of annual rainfall (CVAR). The correlations between indicators were analyzed using R (v. 3.3.1), and the results show a significant correlation between MAP and CVAR ($R = 0.99$) and between the normalized difference water index (NDWI) and normalized differential vegetation index (NDVI) ($R = 0.87$). Based on correlation and standard deviation, CVAR and NDWI were eliminated from the original evaluation system for the landslide susceptibility assessment in the pipeline area (Table 1).

Generally, the evaluation indicator of pipeline vulnerability as it relates to the relationship between a pipeline and its surrounding environment is rarely considered. The evaluation indicators in this paper were refined to include pipeline parameters and the spatial relationship between a pipeline and a landslide. The pipelines in the study area were based in mountainous areas and have been running for many years. All of these pipelines consisted of high-pressure pipes that were made of steel tubes and had a diameter of 610 mm

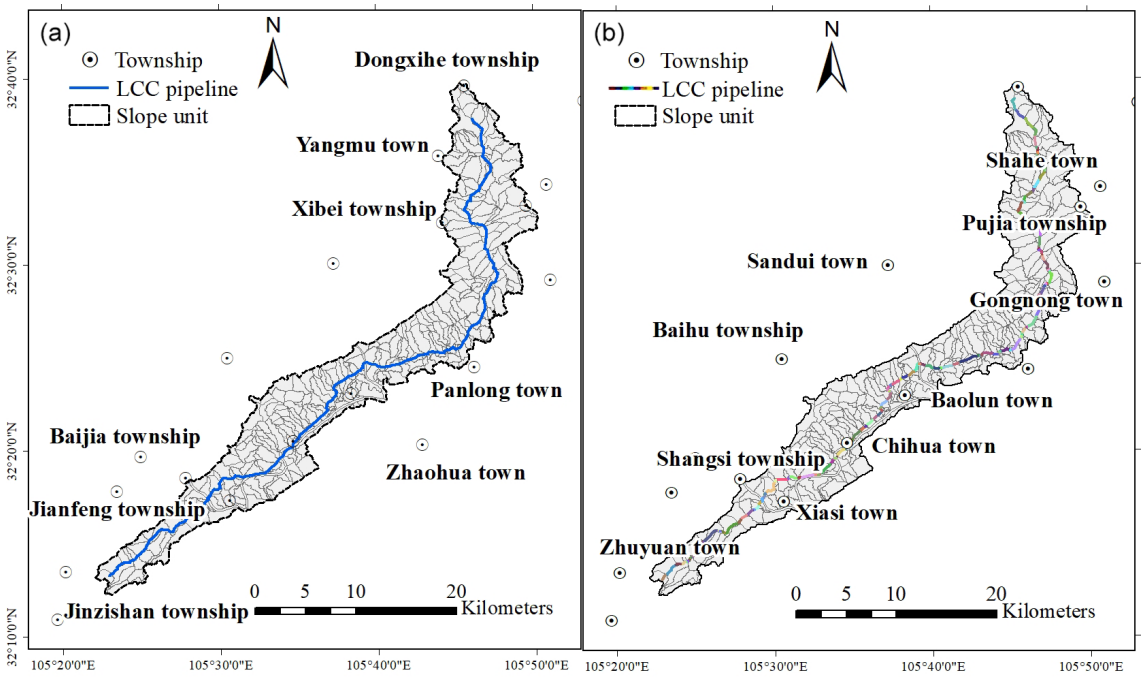

Figure 2. All slope units **(a)** and pipeline sections **(b)** in the study area.

Table 1. Indicators of landslide susceptibility assessment and pipeline vulnerability assessment.

	Factor	Indicators
Landslide hazard indicator	Landform	Elevation Slope Aspect Height difference Topographic profile curvature (TPC)
	Land cover	Normalized differential vegetation index (NDVI) Normalized difference water index (NDWI)
	Geology	Lithology Distance from the fault
	Precipitation	Mean annual precipitation (MAP) Coefficient of variation of annual rainfall (CVAR)
Pipeline vulnerability indicator	Pipe body	Defect density Depth Thickness Pressure Materials Diameter Media
	Spatial relationship between pipeline and landslide	Position Angle

for conveying oil. In keeping with the theory of the entropy weight method, these indicators (e.g., pressure, materials, diameter and media) were not included in the final evaluation system used to determine pipeline vulnerability.

4.3 LM-BP neural network model

A neural network is a nonlinear mathematical structure which is capable of representing complex nonlinear pro-

cesses that relate the inputs and outputs of any system (Hsu et al., 1995). With its good performance in nonlinear statistical modeling, it is very useful in exploring the hidden relationships between the inputs and the outputs (Wu and Wang, 2016). A BP neural network with many adjustable parameters has a powerful parallel processing mechanism, high flexibility and can incorporate uncertainty information well. The mechanism of landslide evaluation is complex with many uncertainties and incomplete information (Jie et al., 2015). The BP neural network model can calculate the intrinsic rules from the vast amount of complex and fuzzy data in the changing environment and make corresponding inferences. The information about landslides reflected by the data used in the process of susceptibility assessment is mostly qualitative rather than quantitative. Through the analysis of this fuzzy information, accurate assessment results can be obtained. Landslide susceptibility assessment is essentially a study of pattern recognition (Feng et al., 2017). The BP neural network can approximate arbitrary continuous function with arbitrary precision, so it is widely used in nonlinear modeling, pattern recognition and pattern classification (Xiong et al., 2010). Because the BP neural network model is widely used, there are many successful cases as a reference for the number of neurons in each layer, the parameters of network learning and the optimization of algorithms, which can effectively improve the reliability and accuracy of the model (Ke and Li, 2014b).

The LM algorithm, also known as the damped least-squares method, has the advantage of local fast convergence. Its strong global searching ability contributes to the strong extrapolation ability of the trained network. The LM algorithm is a combination of the gradient descent method and Gauss–Newton method. Its iteration process is no longer along a single negative gradient direction, which greatly improves the convergence speed and generalization ability of the network (Li et al., 2016). The BP neural network model, optimized by the LM algorithm, was used to evaluate the regional landslide susceptibility in this study. MATLAB 2014 with the *trainlm* training function was used to implement the LM-BP neural network. The flowchart of LM-BP neural network algorithm is shown in Fig. 3.

Data from 106 landslide disasters were collected near the research area. Of these landslides, 23 were within the region of the study area. Most of the landslides located outside the study area were less than 20 km away from the pipeline. Due to comparable environmental conditions, these landslides could still help us identify the relationship between landslides and environment factors. In light of the frequency distribution of each evaluation indicator (Fig. 4), the landslide susceptibility grade corresponding to each interval of the indicators was divided, and then the susceptibility degree monotonicity in each interval was decided. For this study, the landslide susceptibility grade was divided into four levels: low (I), medium (II), high (III) and extremely high (IV). Based on previous research experience and field investigations (Appendix H), the monotonous intervals of different indicators of susceptibility degrees were judged (Appendix A). For instance, there were hardly any landslides, only collapses that occurred in slopes above 60°. Besides, the susceptibility degree in the area was monotone decreasing in the slope interval of 60 to 90°. Because of the very small sliding force in slopes at 0 to 15°, landslides were rare to occur here, even under other extreme conditions (Zhang et al., 2015). On the basis of the classification criteria of the evaluation indicators used to predict landslide susceptibility degree and the functional relationship between the evaluation indicators and landslide probabilities, standard samples (training samples and test samples) were built using a specific mathematical method. When establishing the empty matrix, the sample size of each landslide susceptibility level was set to 200, and the training sample size was 800. According to the order of susceptibility from low to high (Appendix A), the input was constructed by interpolating for each interval. The interval of the susceptibility degree is [0, 1], and the output is obtained by interpolating 800 values equidistantly between the interval of [0, 1] (Appendix B). Using interpolation theory to build samples avoided the excess human influence in the process of building a neural network model by traditional methods. The training samples and test samples were evaluated using similar construction methods but with different sample sizes. Finally, the indicator data were normalized, they were entered into the LM-BP neural network for simulation and 315 slope unit landslide susceptibility values were output.

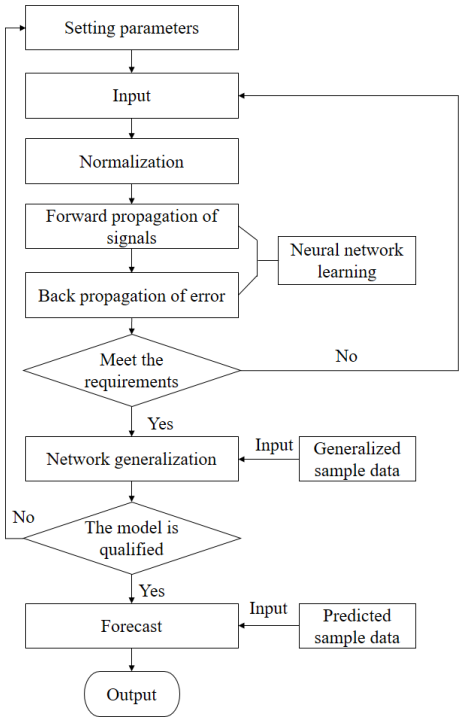

Figure 3. Flowchart of the LM-BP neural network algorithm.

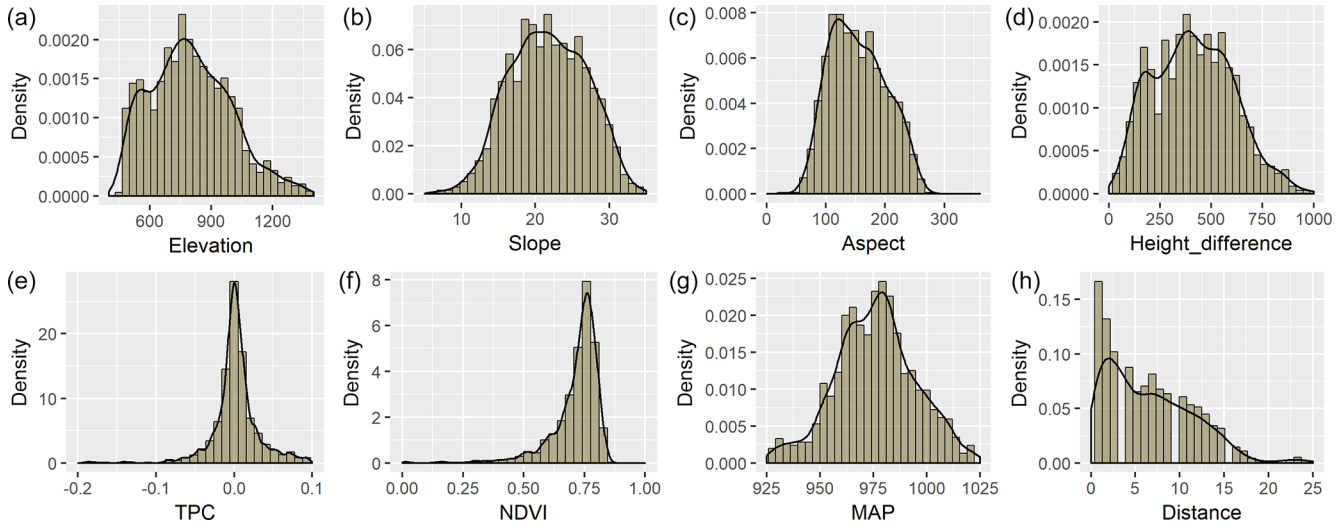

Figure 4. The frequency distribution of each indicator in the landslide location. Maps **(a)**, **(b)**, **(c)**, **(d)**, **(e)**, **(f)**, **(g)** and **(h)** represent the elevation, slope, aspect, height difference, TPC, NDVI, MAP and distance from the fault, respectively.

4.4 Vulnerability assessment model for pipelines

The vulnerability evaluation model of pipelines in the landslide area was established using the entropy weight method, which overcame the shortcomings of the traditional weight method that does not consider the different evaluation indicators and the excessive human influence on the process of evaluation (Gao et al., 2017; Pal, 2014). Entropy is a method of measuring the uncertainty of information by using probability theory (Liu and Zhang, 2011). The entropy indicates the extent of difference in an indicator: the more different the data, the greater the role in evaluation (Jia et al., 2007). The extremum difference method difference method was used to normalize each indicator value. The decision information of each index can be expressed by entropy value e_i:

$$r_{ij} = \frac{x_{ij} - \min_j\{x_{ij}\}}{\max_j\{x_{ij}\} - \min_j\{x_{ij}\}},$$
$$r_{ij} = \frac{\max_j\{x_{ij}\} - x_{ij}}{\max_j\{x_{ij}\} - \min_j\{x_{ij}\}}, \quad (1)$$

$$e_i = \frac{\sum_{j=1}^{n} p\left(x_{ij}\right) \ln p\left(x_{ij}\right)}{\ln(n)}, \quad (2)$$

$$p\left(x_{ij}\right) = \frac{r_{ij}}{\sum_{j=1}^{n} r_{ij}}, \quad (3)$$

$$w_i = \frac{1 - e_i}{m - \sum_{i=1}^{m} e_i}, \quad (4)$$

$$H_j = \sum_{i=1}^{m} w_i r_{ij}, \quad (5)$$

where n is the number of evaluation objects, and r_{ij} represents the ith evaluation indicator values of jth pipe sections. H_j is the evaluation value of the pipeline section's vulnerability; w_i is the weight of the evaluation indicator.

Pipeline defect density was obtained from the pipeline internal inspection data, which consisted of both mileage data that needed to be converted into three-dimensional coordinate data and pipeline centerline coordinate data obtained through C# programming. In addition, the main slide direction of the landslide was replaced by the slope direction that was extracted by the DEM. The coordinate azimuth of the pipe section was extracted using the linear vector data of each pipe section, and the angle between the pipeline and the slope was calculated using the mathematical method. The calculation process was solved in the Visual Basic language on ArcGIS using second development functions. Finally, the entropy weight of 5 indicators was calculated by programming in MATLAB 2014. The entropy weight calculation results for pipeline landslide vulnerability assessment are shown in Table 2.

5 Results and comparison

5.1 Regional landslide susceptibility assessment

The LM-BP neural network was trained and the network was stopped after 182 iterations. An RMSE value of 9.93×10^{-9} indicated that the goal of precision had been reached. Through the simulation of the network test, none of the absolute error values of test data (20 groups) were found to be greater than 0.02; this result aligned with our expectation of the precision of the landslide susceptibility assessment. The landslide susceptibility grade was divided into four levels by

Table 2. Entropy weight of evaluation indicator.

	Depth	Angle	Defect density	Thickness	Position
Weight	0.010007	0.101553	0.678851	0.154322	0.055266
Entropy	0.997322	0.97282	0.818308	0.958696	0.985208

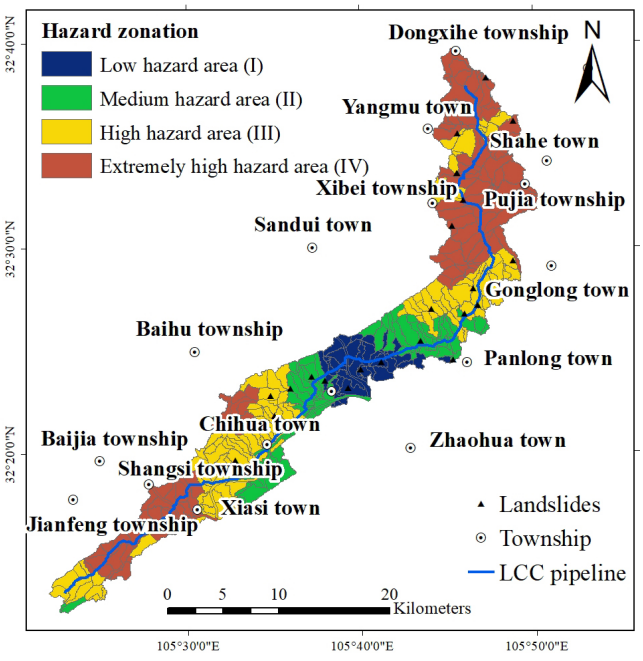

Figure 5. Landslide hazard map of study area.

using the equal interval method at intervals of 0.25. The safe (low-susceptibility) section was located in the central part of the study area. The dangerous (high-susceptibility) section was located north and south (Fig. 5). In the study area, most of the exposed rock was dominated by shale, which belongs to the easy-slip rock group.

Average altitude ranged from 450 to 1400 m, and the relative height difference was greater than 80 m, with the slope between 15 and 35°. Based on an overlay analysis of historic landslides within the study area, and susceptibility zonation maps, we surmised that the probability of landslides in the study area was extremely high, and that 87 % of the landslides occurred in the medium-, high-, and extremely high-susceptibility areas. Among these landslides, three were located in low-susceptibility areas, which accounted for 13 % of the landslide disaster sites, five occurred in medium-susceptibility areas (accounting for 21.7 % of disaster sites), seven occurred in high-susceptibility areas (accounting for 30.4 % of sites) and eight occurred in extremely high-susceptibility areas (accounting for 34.8 % of sites). The evaluation results were found to accurately reflect the trends and rules of distribution of landslides in the study area. The number and area of slopes in high-susceptibility and extremely high-susceptibility areas accounted for about 70 % of the total (Table 3). The probability of landslide occurrence in the study area was generally high, which was consistent with the fact that the region was landslide-prone.

Table 3. Number and area of slopes of four hazard grades.

Landslide susceptibility	Number of slopes	Percentage (%)	Area (km^2)	Percentage (%)
Low (I)	33	10.48	32.63	8.76
Medium (II)	62	19.68	65.53	17.60
High (III)	112	35.56	123.55	33.18
Extremely high (IV)	108	34.29	150.65	40.46
Total	315	100	372.36	100

Table 4. Number and distances of pipeline of four vulnerability grades.

Pipeline vulnerability	Number of pipelines	Percentage (%)	Area (km^2)	Percentage (%)
Low (I)	120	66.66	50.417	62.06
Medium (II)	37	20.56	20.888	25.72
High (III)	22	12.22	9.833	12.11
Extremely high (IV)	1	0.56	0.087	0.11
Total	180	100	81.225	100

5.2 Vulnerability assessment for oil pipeline in landslide area

The equal interval of 0.25 was used to divide the pipeline vulnerability level into four grades to obtain the pipeline vulnerability zonation of the study area (Fig. 6). The pipeline in the northern part of the study area was given a low vulnerability grade, while the situation in the south of the region is more serious. The number, length and percentage of pipeline segments with different grade vulnerabilities are shown in Table 4. The number and length of pipeline segments in highly vulnerable areas (III) and extremely vulnerable areas (IV) accounted for about 12 % of the total.

5.3 Risk assessment for oil pipeline in landslide area

According to natural disaster risk expressions released by the UN, the definition of risk may be expressed as the product of landslide susceptibility in a pipeline area and pipeline vulnerabilities in the landslide area. Scientific analysis and expression of disaster risk assessment results can simplify com-

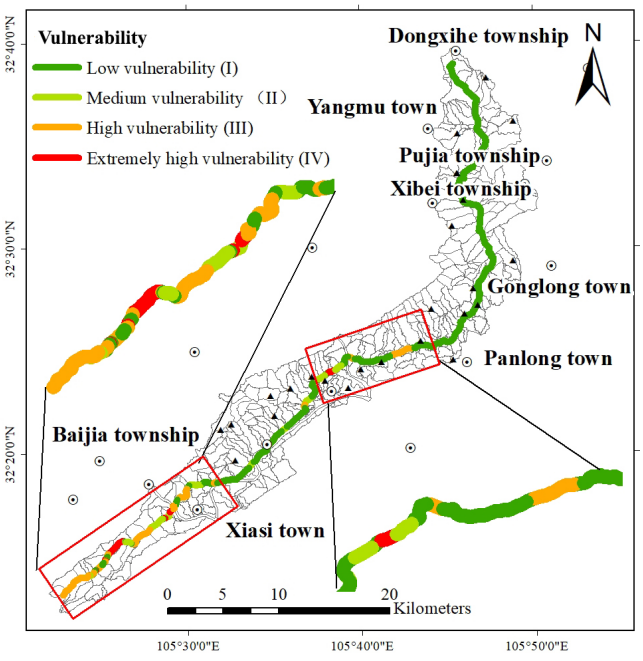

Figure 6. Pipeline vulnerability map of study area.

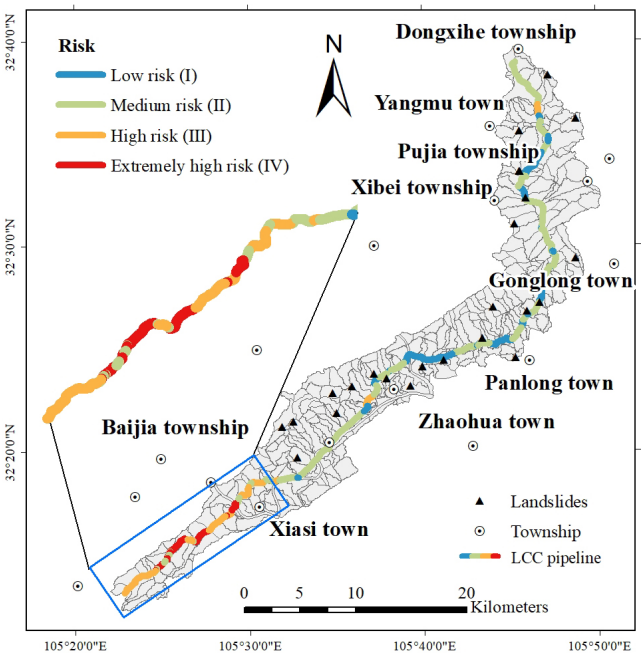

Figure 7. Pipeline risk map of study area.

plex risk assessments and accelerate findings (Ding and Tian, 2013). There is no unified criterion for disaster evaluation zoning, and the equal interval method is one of the methods to express the results more intuitively (Hu et al., 2011; Jin and Meng, 2011; Wang et al., 2011). The susceptibility and vulnerability degrees were distinguished using the equal interval method, and four risk grades were then automatically generated. Where the comprehensive risk assessment value was within 0 to 0.0625, the corresponding risk grade was Grade I; the corresponding risk grades with the values of 0.0625 to 0.25, 0.25 to 0.5625 and 0.5625 to 1.0 were Grade II, III and IV, respectively. The risk grade of each section of the pipeline within the research area is shown in Fig. 7.

The number of sections with a high-risk grade was 33, which accounted for 18.33 % of all pipeline sections and represented 16.57 % of the total pipeline length of 13 461 km. There were four sections with extremely high-risk grade, which accounted for 2.22 % of all sections and represented 3.31 % of the total pipeline length of 2.538 km. The section number and the length of the pipelines lying in high-risk (III) and extremely high-risk (IV) areas accounted for 20 % of the total pipeline length, and the risk grade of pipelines inside Qingchuan and Jian'ge County was relatively high.

5.4 Analysis of risk assessment results

Large or huge landslides were common in areas that we categorized as extremely high risk, which we defined as those that were geologically evolving or had experienced obvious deformations within the last 2 years with cracks that are still visible. These pipelines were subject to dangers at any time, as the pipelines within the areas prone to landslides were found to contain many defects or extensive damage. These areas also posed considerable threats; for example, pipeline ruptures or breaks could lead to leakages or serious deformations that cause transportation failure. Because these are unacceptable events, risk prevention and control measures must be taken as soon as possible. Pipelines with extremely high risk were mainly distributed in the following areas: (1) Xiasi village in Xiasi County (pipe no. K628–K630) and (2) Shiweng village–Maliu village of Xiasi County (pipe no. K635–K637). This section lay in the south of the research area, with an altitude of 500 to 750 m. Here, the slope conditions affected the distribution of groundwater pore pressure and the physical and mechanical characteristics of the rock and soil in three areas: vegetation cover, evaporation and slope erosion. Ultimately, these three factors affected slope stability (Luo and Tan, 2011). Vertical and horizontal ravines were also seen in this section, with a relative height difference greater than 100 m and slopes between 15 to 35°. Slope degrees with obvious changes had a great influence on slope stability (Chang and Kim, 2004; Hu et al., 2015). The exposed rocks in this area were mainly shale and belonged to the sliding-prone rock group. Rock type and interlayer structure were found to be important internal indicators that a landslide could occur (Guzzetti et al., 1996; Xiang et al., 2010; Xin et al., 2009). The distance between the fault and the pipeline in the section was about 2 km with a NDVI of about 0.75 and MAP of about 970 mm. Faulted zones and nearby rock and earth masses that were destroyed in a geologic event reduced the integrity of a slope, and the faults and

important groundwater channels could also cause deformation and damage to a slope (Liu, 2009). The pipelines in these areas exhibited many defects. Most pipelines passed through the slope in an inclined or horizontal way, an attribute that typically increased the risk of a landslide occurring.

In high-risk areas, small or moderate landslides commonly occurred in areas that we have categorized as high risk. They were in the process of deformation, or had obvious deformation recently (within 2 years), such as cracks, subsidence, or tympanites on the landslide, and, in some cases, even shear. The pipelines in these areas had defects and were buried at a shallow depth. If a landslide occurred in this pipeline area, it could cause pipe suspension, floating and damage. It could also contribute to a small to moderate leakage of the multiple petroleum products, such as gasoline, diesel and kerosene. However, damaged pipes can be welded or repaired. Monitoring is critical in high-risk areas. In our study, the pipeline high-risk area was defined as the following areas: (1) Xiasi town–Xiasi village–Shiweng village (pipe no. K622–K633) and (2) Xiasi town–Maliu village–Jinzishan Xiangdasang village (pipe no. K635–K642). This area was located south of the pipe, which was buried in the study area. The altitude of the study area was between 450 and 800 m, the relative elevation difference was over 100 m and the slope was between 15 and 40°. Most of the outcrops in this area were quartz sandstone, which belongs to the easy-sliding rock group. The pipes in this area were about 2.5 km away from faults. The NDVI was about 0.6 to 0.8, and MAP was about 970 nm. Pipes showed many defects, most of them either crossing the slope or lying in the center of slope. All of the above factors provided sufficient conditions for the formation of landslide.

In the medium-risk areas, only small landslides were found to occur, and we observed no sign of deformation. But through the analysis of geological structure, topography and landform, we found the area to demonstrate a tendency for developing landslides. The pipes in this risk area exhibited almost no faults and were buried deep beneath the ground. However, under bad conditions, the landslides in these areas could also affect the pipes' safety, causing the pipes to become exposed or deformed. These areas need simple monitoring. For our study, medium-risk areas were defined as follows: (1) Sanlong village of Dongxihe township–Panlong town–Dongsheng village (pipe no. K559–K593). (2) Panlong town–Qinlao village–Wu'ai village (pipe no. K595–K597). (3) Baolun town–Laolin'gou village–Xiasi town–Youyu village (pipe no. K599–K630).

In the low-risk areas, landslides did not occur under ordinary conditions, but they could occur if a strong earthquake hit or if the area experienced continuous or heavy rain. The pipes in low-risk areas showed no defects and were buried very deep. They were also located far away from areas affected by landslides. Therefore, landslides in these areas caused no obvious damage to the pipes and few threatened the safety of pipes. However, regular inspection is necessary to ensure that the pipes continue to operate safely.

Table 5. Number and distances of pipeline of four risk grades.

Pipeline risk	Number of pipelines	Percentage (%)	Area (km^2)	Percentage (%)
Low (I)	37	20.56	14.469	17.81
Medium (II)	106	58.89	50.757	62.49
High (III)	33	18.33	13.461	16.57
Extremely (IV)	4	2.22	2.538	3.13
Total	180	100	81.225	100

The low-risk areas were defined as follows: (1) Panlong town–Dongsheng village–Qinlao village (pipe no. K591–K597) and (2) Baolun town–Xiaojia village–Baolun town–Laolin'gou village (pipe no. K599–K608).

Through comprehensive analysis of each risk level area, we compiled a list of pipeline landslide risks (Table 6). This list describes each landslide risk level in four respects: pipeline risk, landslide susceptibility, pipeline vulnerability and risk control measures.

The main purpose of this study was to provide managers and planners a comprehensive assessment of landslide risk in areas containing pipelines. The results offer information on the possibility of failure of slopes. The landslide susceptibility maps could help planners reorganize and plan future pipeline construction. Pipeline vulnerability maps could assist engineers in pipeline maintenance operations. Based on this final risk map, managers and engineers can then make decisions and formulate prescriptions that will have highly predictable results for safely transporting petroleum products, relocating settlements and significantly reducing the risk of any adverse effects.

Future research could explore detailed comparison of different methods and recommend one or more optimal approaches. Moreover, This study shows that landslide risk assessments can be performed with a minimal number of relatively easy to obtain datasets. We advocate establishing a database with assessment parameters similar to the one described by this study to construct dynamic landslide risk assessment models.

6 Conclusions

The faults inherent to traditional landslide risk assessments include excessive human influence, failure of pipeline vulnerability assessments to consider the interaction between landslide disaster and pipeline ontology, and the low quantification degree of risk assessment results.

Taking the Guangyuan section (82 km) of the LCC oil and gas pipeline as an example, we used GIS and RS technology to establish a regional landslide susceptibility assessment model based on the LM-BP neural network. We determined that there were 112 and 108 slopes in high-susceptibility and extremely high-susceptibility areas that accounted for

Table 6. Description of pipeline risk level.

Pipeline risk	Landslide susceptibility	Vulnerability	Risk	Control measures
Low (I)	The landslide will not happen under ordinary conditions, but it will occur when strong earthquakes, long-lasting continuous rain or extremely heavy rain occur as well.	The pipes in low-risk areas have no defects and are buried very deeply. Meanwhile, they are far away from the area affected by landslides.	Landslides cause no obvious damage to the pipes and few threats to pipe safety.	Regular inspection
Medium (II)	Small landslides (volume of less than 100 000 m^3) mainly occur with no signs of deformation, but through analyzing geological structures, topography and landforms a tendency for landslides is found.	The pipes have almost no faults and are buried deeply. However, under bad conditions, landslides may also affect pipe safety.	The landslide may cause the pipes to become exposed or deformed.	Simple monitoring
High (III)	Landslides are mostly small to moderate (volume between 100 000 and 1 million m^3), and they are in deformations or have recently had obvious deformation, such as cracks, subsidence, or tympanites on the landslide, and, in some cases, even shear	The pipeline has defects and is buried shallowly. Once landslides occur in the pipeline area, pipe safety will be threatened.	The safety of pipeline will be threatened and may suffer from pipe suspension, floating and damage, etc. Therefore, it will contribute to a small amount of petroleum product leakage. Fortunately, the pipe can be welded or repaired.	Intensive monitoring
Extremely high (IV)	Large (volume between 1 million and 10 million m^3) or huge (volume greater than 10 million m^3) landslides are common in the areas with extremely high risk, which are changing or have experienced obvious deformation recently with visible cracks.	The pipelines are subject to dangers at any time as the pipelines within the area prone to landslides have been observed as having many defects or a lot of damage.	There are extreme dangers, for example pipeline rupture or break, and these may lead to considerable leakage of multiple petroleum products or serious deformation and even interruption of oil and gas transportation.	Prevention and control measures should be taken as soon as possible.

33.18 % and 40.46 % of the total area of the study area, respectively. Then, we established the model of pipeline vulnerability evaluation based on the entropy weight method by combining the pipeline body and the environmental information. The number and length of pipe segments in the highly vulnerable (III) and extremely vulnerable areas (IV) accounted for about 12 % of the total. Finally, based on the susceptibility assessment and the vulnerability assessment, we completed the risk assessment and risk division of the oil pipeline, thus forming a geological disaster risk assessment model and a method for oil pipeline and landslide risk assessment. The risk assessment results demonstrated that the number and length of high-susceptibility and extremely high-susceptibility pipeline segments represented 20 % of the total. Similarly, the pipeline risk within Qingchuan and Jian'ge counties was relatively high. Our pipeline landslide risk assessment has laid a foundation for the future study of pipeline safety management and pipeline failure consequence loss assessment.

Data availability. DEM data can be downloaded from the Geospatial Data Cloud (http://www.gscloud.cn/, last access: October 2016). Precipitation data (dataset of annual surface observation values in China between the years 1981 and 2010) are provided by China Meteorological Administration (http://data.cma.cn/, last access: January 2017). Geological maps, landslide data and pipeline mileage data can be requested by email from the author at neu_xjn@163.com.

Appendix A

Table A1. Classification of landslide susceptibility grade corresponding to different intervals.

Factor	Indicators	Interval	Susceptibility degree monotonicity	Susceptibility level
Landform	Elevation	[1000, highest]	Decreasing	Low susceptibility (I)
		[Lowest, 600)	Increasing	Medium susceptibility (II)
		[800, 1000)	Decreasing	High susceptibility (III)
		[600, 700) ∪ [700, 800)	Increasing, decreasing	Extremely high susceptibility (IV)
	Slope	[60, 90)	Decreasing	Low susceptibility (I)
		[0, 15)	Increasing	Medium susceptibility (II)
		[30, 60)	Decreasing	High susceptibility (III)
		[15, 20) ∪ [20, 30)	Increasing, decreasing	Extremely high susceptibility (IV)
	Aspect	[0, 45) ∪ [270, 360)	Increasing, decreasing	Low susceptibility (I)
		[225, 270) ∪ [45, 90)	Decreasing, increasing	Medium susceptibility (II)
		[90, 135) ∪ [180, 225)	Increasing, decreasing	High susceptibility (III)
		[135, 157.5) ∪ [157.5, 180)	Increasing, decreasing	Extremely high susceptibility (IV)
	Height difference	[Lowest, 100)	Increasing	Low susceptibility (I)
		[900, highest] ∪ [100, 200)	Decreasing, increasing	Medium susceptibility (II)
		[600, 900) ∪ [200, 300)	Decreasing, increasing	High susceptibility (III)
		[300, 450) ∪ [450, 600)	Increasing, decreasing	Extremely high susceptibility (IV)
	Topographic profile curvature	[Lowest, −0.025)	Increasing	Low susceptibility (I)
		[0.025, highest]	Decreasing	Medium susceptibility (II)
		[−0.025, −0.01) ∪ [0.01, 0.025)	Increasing, decreasing	High susceptibility (III)
		[−0.01, 0) ∪ [0, 0.01)	Increasing, decreasing	Extremely high susceptibility (IV)
Land cover	NDVI	[−1, 0)	Increasing	Low susceptibility (I)
		[0, 0.6) ∪ [0.9, 1]	Increasing, decreasing	Medium susceptibility (II)
		[0.6, 0.7) ∪ [0.8, 0.9)	Increasing, decreasing	High susceptibility (III)
		[0.7, 0.75) ∪ [0.75, 0.8)	Increasing, decreasing	Extremely high susceptibility (IV)
Precipitation	Mean annual precipitation	[1100, highest)	Decreasing	Low susceptibility (I)
		[Lowest, 960)	Increasing	Medium susceptibility (II)
		[990, 1100)	Decreasing	High susceptibility (III)
		[960, 975) ∪ [975, 990)	Increasing, decreasing	Extremely high susceptibility (IV)
Geology	Distance from the fault	[20, highest]	Decreasing	Low susceptibility (I)
		[15, 20)	Decreasing	Medium susceptibility (II)
		[5, 15)	Decreasing	High susceptibility (III)
		[0, 5)	Decreasing	Extremely high susceptibility (IV)

Appendix B

Table B1. Standard training sample matrix and standard test sample matrix.

Sample type	ID	Input									Output
		Aspect	Slope	Elevation	NDVI	MAP	Height difference	TPC	Distance	Lithology	
Training sample	1	0.2	89.9	438	−1	908.1	33	−0.582	25	1	0
	50	35.2	82.8	453	0	912.2	79	−0.456	23.47	1	0.06
	100	297.1	75.7	469	0.88	916.3	115	−0.33	21.9	1	0.12
	150	329.3	67.6	485	0.95	920.4	167	−0.168	20.34	1	0.19
	200	359.5	60	499	1	924.9	200	0.628	18.77	1	0.25
	250	68.4	3.8	1293	0.73	930.4	1097	0.486	17.21	2	0.31
	300	89.3	8.2	1206	0.65	938	1039	0.326	15.64	2	0.37
	350	246	12	1102	0.56	943.6	977	0.183	14.08	2	0.44
	400	269.3	15	1002	0.5	949.8	902	−0.142	12.52	2	0.5
	450	113.4	52.9	952	0.46	960.6	848	−0.018	10.95	3	0.56
	500	134.8	46.3	905	0.4	972.6	757	−0.012	9.39	3	0.62
Test sample	1	27.2	72.3	458	0.8	911.6	59	−0.544	25	1	0
	2	28.5	71.6	468	0.81	914.3	74	−0.453	23.69	1	0.06
	3	31.5	69.5	488	0.85	915.8	86	−0.381	22.37	1	0.11
	4	37.8	66.2	490	0.86	917.1	100	−0.228	21.06	1	0.16
	5	38.6	62.1	497	0.86	919.1	152	−0.03	19.74	1	0.22
	6	56.1	4.4	1141	0.7	934.2	939	0.439	18.43	2	0.27
	7	57.3	6.6	1240	0.68	939.6	941	0.429	17.11	2	0.32
	8	65.3	9.8	1257	0.66	945.1	1124	0.413	15.79	2	0.37
	9	68.2	11	1290	0.56	948.8	1135	0.318	14.48	2	0.43
	10	74.7	11.9	1382	0.53	949.9	1146	0.148	13.16	2	0.48
	11	92.4	30.4	848	0.47	963.4	613	−0.019	11.85	3	0.53
	12	92.7	31.8	853	0.45	970.5	683	−0.016	10.53	3	0.58
	13	101.9	44.7	900	0.45	980.5	737	−0.015	9.22	3	0.64
	14	110.1	50.9	917	0.35	987	817	−0.015	7.9	3	0.69
	15	115.6	57.5	933	0.32	994.2	835	−0.015	6.58	3	0.74
	16	140.6	15.6	502	0.14	1001.5	245	0.019	5.27	4	0.79
	17	155.4	20	626	0.14	1002.3	256	0.008	3.95	4	0.85
	18	157.1	24.8	690	0.08	1010.6	293	0.007	2.64	4	0.9
	19	177.6	27.3	765	0.06	1012.7	392	0.004	1.32	4	0.95
	20	178.3	29.6	795	0.04	1022.7	446	0.001	0	4	1

Appendix C

Table C1. Test error of LM-BP neural network.

Number	Expected value	Network output	Error
1	0	0.0006	0.0006
2	0.06	0.0548	−0.0052
3	0.11	0.1113	0.0013
4	0.16	0.1699	0.0099
5	0.22	0.2302	0.0102
6	0.27	0.2614	−0.0086
7	0.32	0.315	−0.005
8	0.37	0.3697	−0.0003
9	0.43	0.4266	−0.0034
10	0.48	0.4899	0.0099
11	0.53	0.5153	−0.0147
12	0.58	0.5765	−0.0035
13	0.64	0.6405	0.0005
14	0.69	0.701	0.011
15	0.74	0.7523	0.0123
16	0.79	0.8094	0.0194
17	0.85	0.8616	0.0116
18	0.9	0.9155	0.0155
19	0.95	0.9675	0.0175
20	1	1.0173	0.0173

Appendix D

Table D1. Coordinates of the centerline and ancillary facilities of the pipeline. Secrecy regulations regarding geographical coordinate data in the People's Republic of China stipulate that the first three digits of each location's coordinates remain confidential. In this table, this has been represented by ellipses.

Point number	Previous point	Material	Diameter	Pressure	Depth	Coordinate			Elevation
			(mm)		(m)	X	Y	H	
Marker peg		–	–	–	–	···576.265	···4357.849	503.877	–
GD1.421	GD1.420	Steel	168	high	2.2	···572.111	···4352.109	504.235	502.035
GD1.422	GD1.421	Steel	168	high	1.9	···571.837	···4336.010	503.866	501.966
GD1.423	GD1.422	Steel	168	high	2.1	···571.538	···4319.679	503.694	501.594
GD1.424	GD1.423	Steel	168	high	2.1	···571.093	···4308.825	503.510	501.410
GD1.425	GD1.424	Steel	168	high	2.0	···570.718	···4288.141	503.733	501.733
Detective pole K566		–	–	–	–	···575.536	···4284.069	503.494	–
GD1.426	GD1.425	Steel	168	high	2.3	···570.603	···4275.147		
Mileage peg K566+200		–	–	–	–	···574.641	···4258.41	503.224	–
GD1.427	GD1.426	Steel	168	high	2.0	···570.222	···4258.593	503.710	501.710
GD1.428	GD1.427	Steel	168	high	1.6	···570.090	···4247.642	503.283	501.683
GD1.429	GD1.428	Steel	168	high	2.3	···569.458	···4216.618	502.468	500.168
GD1.430	GD1.429	Steel	168	high	2.9	···569.043	···4208.558	504.055	501.155

Appendix E

Table E1. Internal detection data of each pipeline.

Feature ID	Pipe number	Distance (m)	Feature type	Remarks	Length (mm)	Thickness (mm)
1	10	6.408	Pipe segment	Spiral weld	652	11.1
2	20	7.060	Pipe segment	–	1178	–
3	20	7.648	Fixed punctuation point	Valve centerline	–	–
4	20	7.650	Valve	Centerline	–	–
5	30	8.238	Pipe segment	Spiral weld	768	11.1
6	40	9.006	Pipe segment	–	2184	–
7	40	10.100	Globular tee	Centerline	–	–
8	50	11.190	Pipe segment	Spiral weld	1700	11.1
9	50	11.445	Pit	–	548	11.1
10	60	12.890	Pipe segment	Straight weld	2342	13.6
11	60	12.890	Wall thickness variation	from 11.1 to 13.6 mm	–	–
13	70	15.232	Pipe segment	Spiral weld	1999	11.1
14	70	15.232	Wall thickness variation	From 13.6 to 11.1 mm	–	–
15	80	17.231	Pipe segment	Straight weld	2352	13.4
16	80	17.231	Wall thickness variation	From 11.1 to 13.4 mm	–	–
18	90	19.583	Pipe segment	Spiral weld	11 557	11.1
19	90	19.583	Wall thickness variation	From 13.4 to 11.1 mm	–	–
20	90	28.060	Attachments	–	598	11.1
21	100	31.140	Pipe segment	–	991	–
22	100	31.580	Flange	centerline	–	–
23	110	32.131	Pipe segment	Spiral weld	11 660	11.1
24	120	43.791	Pipe segment	Spiral weld	5536	11.1
25	130	49.327	Pipe segment	Straight weld	2213	16.2
26	130	49.327	Wall thickness variation	From 11.1 to 16.2 mm	–	–
28	140	51.540	Pipe segment	Spiral weld	5608	11.1
29	140	51.540	Wall thickness variation	From 16.2 to 11.1 mm	–	–
30	150	57.148	Pipe segment	Spiral weld	9432	11.1

Appendix F: Core code of pipeline defect point coordinate calculating program

```
using System;
using System.Collections.Generic;
using System.ComponentModel;
using System.Data;
using System.Drawing;
using System.Linq;
using System.Text;
using System.Threading.Tasks;
using System.Windows.Forms;
using System.IO;
private void button10_Click(object sender, EventArgs e)
{
    double x1 = 0, y1 = 0, z1 = 0, x2 = 0, y2 = 0, z2 = 0, d1 = 0, d2 = 0, h1 = 0, h2 = 0;
    double l = Convert.ToDouble(textBox9.Text);
    double f = 0,nl=Convert.ToDouble(textBox7 .Text );
    string[] SplitTxt = textBox2.Text.Split(',');
    for (long    i = 0; i < SplitTxt.Length-9; i+=5)
    {
        d1 = Convert.ToDouble(SplitTxt[i + 1]);
        x1 = Convert.ToDouble(SplitTxt[i + 2]);
        y1 = Convert.ToDouble(SplitTxt[i + 3]);
        z1 = Convert.ToDouble(SplitTxt[i + 4]);
        d2 = Convert.ToDouble(SplitTxt[i + 6]);
        x2 = Convert.ToDouble(SplitTxt[i + 7]);
        y2 = Convert.ToDouble(SplitTxt[i + 8]);
        z2 = Convert.ToDouble(SplitTxt[i + 9]);
        h1 = z1-d1;
        h2 = z2-d2;
        l += Math.Sqrt((x1-x2)*(x1-x2)+(y1-y2)*(y1-y2)+(h1-h2)*(h1-h2));
    }
        textBox8.Text =l.ToString();
        f = (nl-l)/nl;
        ff = f;
        textBox5.Text = Convert.ToDouble(f ).ToString("P");
}
private void button9_Click(object sender, EventArgs e)
{
    double f1 = ff ;
    double l1 = 0;
    string zb = "";    string[] SplitTxt = textBox3.Text.Split(',');
    for (long i = 0; i < SplitTxt.Length - 1; i += 2)
    {
        l1 = Convert.ToDouble(SplitTxt[i + 1]);
```

```
            l1 += (-ff) * l1;
            double x1 = 0, y1 = 0, z1 = 0, x2 = 0, y2 = 0, z2 = 0, d1 = 0, d2 = 0, h1 = 0, h2 = 0,
    l0=0,l2=0;
            double l = Convert.ToDouble(textBox9.Text);
            double x = 0, y = 0, h = 0;
            string[] SplitTxt1 = textBox2.Text.Split(',');
            for (long j = 0; j < SplitTxt1.Length - 9; j += 5)
            {
                d1 = Convert.ToDouble(SplitTxt1[j    + 1]);
                x1 = Convert.ToDouble(SplitTxt1[j    + 2]);
                y1 = Convert.ToDouble(SplitTxt1[j    + 3]);
                z1 = Convert.ToDouble(SplitTxt1[j    + 4]);
                d2 = Convert.ToDouble(SplitTxt1[j    + 6]);
                x2 = Convert.ToDouble(SplitTxt1[j    + 7]);
                y2 = Convert.ToDouble(SplitTxt1[j    + 8]);
                z2 = Convert.ToDouble(SplitTxt1[j    + 9]);
                h1 = z1 - d1; h2 = z2 - d2;
                l0= Math.Sqrt((x1 - x2) * (x1 - x2) + (y1 - y2) * (y1 - y2) + (h1 - h2) * (h1 - h2));
                l = l + l0;
                if (l - l1 < 0)
                {
                    ;
                }
                else if (l - l1 >0)
                {
                    l2 = l0 - (l - l1);
                    x = x1 + (x2 - x1) * l2 / l0;
                    y = y1 + (y2 - y1) * l2 / l0;
                    h = h1 + (h2 - h1) * l2 / l0;
                    string xx, yy, hh, v;
                    v = SplitTxt[i];
                    xx = Convert.ToDouble(x).ToString();
                    yy = Convert.ToDouble(y).ToString();
                    hh = Convert.ToDouble(h).ToString();
                    zb    +=v + ","+ xx    + "," + yy + "," + hh +",\n";
                    break;
                }
            }
        }
                textBox6.Text = zb;
    }
```

Appendix G

Table G1. Pipeline landslide risk assessment results.

FID	Start	Terminus	Susceptibility	Susceptibility level	Vulnerability	Vulnerability level	Risk	Risk level
1	K558	K559+446	0.874	IV	0.168	I	0.147	II
2	K559+446	K563+718	0.874	IV	0.178	I	0.156	II
3	K563+718	K564+883	0.932	IV	0.143	I	0.133	II
4	K564+883	K566+90	0.943	IV	0.149	I	0.141	II
5	K566+90	K567+117	0.943	IV	0.280	II	0.264	III
6	K567+117	K567+224	0.766	IV	0.095	I	0.073	I
7	K567+224	K567+384	0.729	III	0.117	I	0.085	II
8	K567+384	K567+674	0.729	III	0.079	I	0.058	I
9	K567+674	K567+782	0.729	III	0.141	I	0.103	II
10	K567+782	K567+846	0.729	III	0.066	I	0.048	I
11	K567+846	K567+904	0.729	III	0.097	I	0.071	I
12	K568+904	K568+197	0.722	III	0.154	I	0.111	II
13	K568+197	K568+430	0.763	IV	0.144	I	0.110	II
14	K569+430	K569+419	0.739	III	0.186	I	0.137	II
15	K569+419	K569+443	0.739	III	0.141	I	0.104	II
16	K569+443	K569+467	0.739	III	0.107	I	0.079	II
17	K569+467	K569+578	0.739	III	0.121	I	0.089	II
18	K569+578	K569+920	0.739	III	0.107	I	0.079	II
19	K571+920	K571+123	0.736	III	0.127	I	0.093	II
20	K571+123	K571+982	0.799	IV	0.109	I	0.087	II
21	K572+982	K572+729	0.753	IV	0.090	I	0.068	I
22	K573+729	K573+548	0.802	IV	0.094	I	0.075	I
23	K574+548	K574+249	0.805	IV	0.084	I	0.068	I
24	K574+249	K574+525	0.805	IV	0.150	I	0.121	II
25	K575+525	K575+538	0.805	IV	0.115	I	0.093	II
26	K575+538	K575+600	0.805	IV	0.157	I	0.126	II
27	K576+600	K576+737	0.816	IV	0.108	I	0.088	II
28	K577+737	K577+120	0.889	IV	0.089	I	0.079	I
29	K577+120	K577+146	0.889	IV	0.094	I	0.084	I
30	K577+146	K577+187	0.889	IV	0.169	I	0.150	II
31	K578+187	K578+571	0.889	IV	0.118	I	0.105	II
32	K578+571	K578+608	0.889	IV	0.095	I	0.084	I
33	K579+608	K579+624	0.853	IV	0.133	I	0.113	II
34	K580+624	K580+582	0.871	IV	0.156	I	0.136	II
35	K581+582	K581+43	0.871	IV	0.097	I	0.084	I
36	K581+43	K581+273	0.871	IV	0.143	I	0.125	II
37	K581+273	K581+536	0.880	IV	0.125	I	0.110	II
38	K581+536	K581+659	0.872	IV	0.154	I	0.134	II
39	K582+659	K582+263	0.830	IV	0.152	I	0.126	II
40	K582+263	K582+437	0.830	IV	0.116	I	0.096	II
41	K583+437	K583+512	0.830	IV	0.152	I	0.126	II
42	K583+512	K583+693	0.798	IV	0.105	I	0.084	II
43	K583+693	K583+720	0.740	III	0.113	I	0.084	II
44	K585+720	K585+55	0.740	III	0.178	I	0.132	II
45	K585+55	K585+101	0.668	III	0.196	I	0.131	II
46	K585+101	K585+370	0.668	III	0.178	I	0.119	II
47	K585+370	K585+634	0.696	III	0.190	I	0.132	II
48	K585+634	K585+734	0.668	III	0.116	I	0.077	II
49	K585+734	K585+908	0.627	III	0.198	I	0.124	II
50	K585+908	K585+949	0.627	III	0.168	I	0.105	II

Table G1. Continued.

FID	Start	Terminus	Susceptibility	Susceptibility level	Vulnerability	Vulnerability level	Risk	Risk level
51	K586+949	K586+782	0.627	III	0.173	I	0.108	II
52	K586+782	K586+805	0.627	III	0.117	I	0.073	II
53	K587+805	K587+364	0.627	III	0.171	I	0.107	II
54	K587+364	K587+498	0.618	III	0.078	I	0.048	I
55	K587+498	K587+794	0.618	III	0.107	I	0.066	I
56	K589+794	K589+251	0.618	III	0.102	I	0.063	I
57	K590+251	K590+757	0.618	III	0.172	I	0.106	II
58	K590+757	K590+780	0.556	III	0.153	I	0.085	II
59	K590+780	K590+812	0.556	III	0.123	I	0.068	II
60	K591+812	K591+500	0.555	III	0.135	I	0.075	II
61	K591+500	K591+946	0.555	III	0.087	I	0.048	I
62	K592+946	K592+259	0.555	III	0.107	I	0.059	I
63	K593+259	K593+631	0.517	III	0.152	I	0.079	II
64	K593+631	K593+912	0.374	II	0.153	I	0.057	II
65	K594+912	K594+993	0.374	II	0.150	I	0.056	II
66	K595+993	K595+203	0.374	II	0.076	I	0.028	I
67	K595+203	K595+261	0.359	II	0.114	I	0.041	I
68	K595+261	K595+383	0.359	II	0.099	I	0.036	I
69	K596+383	K596+383	0.412	II	0.278	II	0.115	II
70	K596+383	K596+429	0.412	II	0.107	I	0.044	I
71	K597+429	K597+62	0.359	II	0.121	I	0.043	I
72	K597+62	K597+200	0.412	II	0.158	I	0.065	II
73	K597+200	K597+345	0.412	II	0.133	I	0.055	I
74	K597+345	K597+680	0.412	II	0.273	II	0.112	II
75	K599+680	K599+376	0.321	II	0.461	II	0.148	II
76	K599+376	K599+693	0.211	I	0.105	I	0.022	I
77	K600+693	K600+188	0.211	I	0.179	I	0.038	I
78	K600+188	K600+353	0.106	I	0.172	I	0.018	I
79	K601+353	K601+369	0.106	I	0.264	II	0.028	I
80	K602+369	K602+495	0.099	I	0.190	I	0.019	I
81	K603+495	K603+131	0.067	I	0.436	II	0.029	I
82	K603+131	K603+551	0.099	I	0.144	I	0.014	I
83	K604+551	K604+321	0.104	I	0.253	II	0.026	I
84	K604+321	K604+976	0.099	I	0.102	I	0.010	I
85	K605+976	K605+735	0.178	I	0.372	II	0.066	II
86	K606+735	K606+368	0.236	I	0.637	III	0.150	II
87	K606+368	K606+838	0.236	I	0.127	I	0.030	I
88	K607+838	K607+596	0.323	II	0.407	II	0.131	II
89	K608+596	K608+20	0.323	II	0.163	I	0.053	II
90	K608+20	K608+287	0.323	II	0.145	I	0.047	I
91	K608+287	K608+546	0.346	II	0.084	I	0.029	I
92	K608+546	K608+583	0.406	II	0.215	I	0.087	II
93	K608+583	K608+835	0.406	II	0.291	II	0.118	II
94	K609+835	K609+565	0.442	II	0.279	II	0.123	II
95	K610+565	K610+564	0.442	II	0.403	II	0.178	II
96	K610+564	K610+945	0.442	II	0.453	II	0.200	II
97	K611+945	K611+89	0.482	II	0.117	I	0.056	I
98	K611+89	K611+691	0.501	III	0.138	I	0.069	II
99	K612+691	K612+413	0.501	III	0.175	I	0.088	II
100	K613+413	K613+269	0.501	III	0.163	I	0.082	II
101	K613+269	K613+442	0.502	III	0.166	I	0.083	II
102	K614+442	K614+83	0.502	III	0.354	II	0.178	II
103	K614+83	K614+980	0.502	III	0.263	II	0.132	II
104	K615+980	K615+218	0.601	III	0.153	I	0.092	II

Table G1. Continued.

FID	Start	Terminus	Susceptibility	Susceptibility level	Vulnerability	Vulnerability level	Risk	Risk level
105	K615+218	K615+388	0.601	III	0.143	I	0.086	II
106	K616+388	K616+87	0.635	III	0.126	I	0.080	II
107	K616+87	K616+300	0.556	III	0.144	I	0.080	II
108	K616+300	K616+460	0.505	III	0.269	II	0.136	II
109	K617+460	K617+715	0.505	III	0.172	I	0.087	II
110	K617+715	K617+827	0.505	III	0.255	II	0.129	II
111	K618+827	K618+28	0.556	III	0.170	I	0.095	II
112	K618+28	K618+687	0.556	III	0.313	II	0.174	II
113	K620+687	K620+78	0.556	III	0.188	I	0.105	II
114	K620+78	K620+298	0.425	II	0.196	I	0.083	II
115	K621+298	K621+509	0.576	III	0.223	I	0.128	II
116	K621+509	K621+611	0.425	II	0.107	I	0.045	I
117	K622+611	K622+10	0.425	II	0.262	II	0.111	II
118	K622+10	K622+86	0.425	II	0.122	I	0.052	I
119	K622+86	K622+539	0.693	III	0.178	I	0.123	II
120	K622+539	K622+897	0.634	III	0.549	III	0.348	III
121	K623+897	K623+36	0.634	III	0.535	III	0.339	III
122	K623+36	K623+794	0.693	III	0.145	I	0.100	II
123	K624+794	K624+866	0.693	III	0.310	II	0.215	II
124	K625+866	K625+242	0.796	IV	0.137	I	0.109	II
125	K627+242	K627+60	0.859	IV	0.452	II	0.388	III
126	K627+60	K627+162	0.859	IV	0.193	I	0.166	II
127	K627+162	K627+313	0.859	IV	0.166	I	0.143	II
128	K627+313	K627+700	0.783	IV	0.167	I	0.131	II
129	K628+700	K628+146	0.908	IV	0.501	III	0.455	III
130	K628+146	K628+196	0.908	IV	0.139	I	0.126	II
131	K628+196	K628+610	0.908	IV	0.631	III	0.573	IV
132	K629+610	K629+355	0.787	IV	0.369	II	0.290	III
133	K629+355	K629+525	0.787	IV	0.729	III	0.574	IV
134	K629+525	K629+570	0.787	IV	0.252	II	0.198	II
135	K629+570	K629+620	0.787	IV	0.465	II	0.366	III
136	K630+620	K630+348	0.787	IV	0.286	II	0.225	II
137	K630+348	K630+956	0.892	IV	0.389	II	0.347	III
138	K631+956	K631+116	0.886	IV	0.423	II	0.375	III
139	K631+116	K631+528	0.805	IV	0.513	III	0.413	III
140	K633+528	K633+435	0.805	IV	0.568	III	0.457	III
141	K635+435	K635+302	0.933	IV	0.625	III	0.583	IV
142	K635+302	K635+326	0.884	IV	0.611	III	0.540	III
143	K635+326	K635+359	0.884	IV	0.441	II	0.390	III
144	K635+359	K635+368	0.884	IV	0.194	I	0.171	II
145	K635+368	K635+530	0.884	IV	0.374	II	0.331	III
146	K635+530	K635+604	0.884	IV	0.307	II	0.271	III
147	K635+604	K635+850	0.805	IV	0.377	II	0.303	III
148	K635+850	K635+943	0.805	IV	0.234	I	0.188	II
149	K635+943	K635+972	0.805	IV	0.139	I	0.112	II
150	K635+972	K635+974	0.805	IV	0.121	I	0.097	II
151	K635+974	K635+990	0.805	IV	0.138	I	0.111	II
152	K636+990	K636+152	0.933	IV	0.598	III	0.558	III
153	K636+152	K636+159	0.933	IV	0.157	I	0.146	II
154	K636+159	K636+320	0.884	IV	0.579	III	0.512	III
155	K636+320	K636+427	0.884	IV	0.166	I	0.147	II
156	K636+427	K636+517	0.884	IV	0.124	I	0.110	II
157	K636+517	K636+806	0.834	IV	0.663	III	0.553	III
158	K636+806	K636+893	0.834	IV	0.794	IV	0.662	IV

Table G1. Continued.

FID	Start	Terminus	Susceptibility	Susceptibility level	Vulnerability	Vulnerability level	Risk	Risk level
159	K637+893	K637+57	0.834	IV	0.519	III	0.433	III
160	K637+57	K637+109	0.834	IV	0.542	III	0.452	III
161	K637+109	K637+181	0.834	IV	0.111	I	0.093	II
162	K637+181	K637+332	0.834	IV	0.127	I	0.106	II
163	K638+332	K638+87	0.834	IV	0.608	III	0.507	III
164	K638+87	K638+140	0.834	IV	0.157	I	0.131	II
165	K638+140	K638+193	0.767	IV	0.682	III	0.523	III
166	K638+193	K638+199	0.767	IV	0.188	I	0.144	II
167	K638+199	K638+226	0.767	IV	0.126	I	0.097	II
168	K638+226	K638+368	0.767	IV	0.532	III	0.408	III
169	K638+368	K638+409	0.767	IV	0.604	III	0.463	III
170	K638+409	K638+432	0.767	IV	0.205	I	0.157	II
171	K638+432	K638+444	0.767	IV	0.525	III	0.403	III
172	K638+444	K638+676	0.767	IV	0.173	I	0.133	II
173	K638+676	K638+837	0.767	IV	0.479	II	0.367	III
174	K639+837	K639+266	0.744	III	0.483	II	0.359	III
175	K639+266	K639+339	0.744	III	0.427	II	0.318	III
176	K639+339	K639+435	0.744	III	0.549	III	0.408	III
177	K639+435	K639+562	0.631	III	0.324	II	0.204	II
178	K640+562	K640+63	0.607	III	0.476	II	0.289	III
179	K641+63	K641+600	0.607	III	0.604	III	0.367	III
180	K642+600	K642+225	0.607	III	0.461	II	0.280	III

Appendix H: Field environment of study area

Figure H1. Vegetation distribution in a watershed in the study area.

Figure H2. Vegetation environment of a pipeline section in the study area.

Figure H3. Outcropping of rock strata in the study area.

Author contributions. JX conceived and designed the experiments, MS performed the experiments and analyzed the data, HZ wrote the paper and WC helped to prepare the paper. YY helped edit language and MS, YC and JW helped draw the maps. All authors read and approved the final paper.

Competing interests. The authors declare that they have no conflict of interest.

Special issue statement. This article is part of the special issue "Advances in computational modelling of natural hazards and geohazards".

Acknowledgements. The study has been funded by the Strategic Priority Research Program of Chinese Academy of Sciences (XDA20030302), IWHR (China Institute of Water Resources and Hydropower Research) National Mountain Flood Disaster Investigation Project (SHZH-IWHR-57), Scientific and Technological Innovation Team Project of Southwest Petroleum University (2017CXTD09) and the Open Topic of Digital Fujian Institute of Large Data for Natural Disaster Monitoring (NDMBD2018003).

Edited by: Albert J. Kettner
Reviewed by: two anonymous referees

References

Akgun, A., Kıncal, C., and Pradhan, B.: Application of remote sensing data and GIS for landslide risk assessment as an environmental threat to Izmir city (west Turkey), Environ. Monit. Assess., 184, 5453–5470, https://doi.org/10.1007/s10661-011-2352-8, 2012.

Atta-Ur-Rahman and Shaw, R.: Hazard, Vulnerability and Risk: The Pakistan Context, Springer, Japan, 2015.

Avalon Cullen, C., Al-Suhili, R., and Khanbilvardi, R.: Guidance Index for Shallow Landslide Hazard Analysis, Remote. Sens., 8, 866, https://doi.org/10.3390/rs8100866, 2016.

Chang, H. and Kim, N. K.: The evaluation and the sensitivity analysis of GIS-based landslide susceptibility models, Geosci. J., 8, 415–423, https://doi.org/10.1007/BF02910477, 2004.

Ding, M. and Tian, S.: Landslide and Debris Flow Risk Assessment and Its Application, Science Press, Beijing, 2013.

Ding, M., Heiser, M., Hübl, J., and Fuchs, S.: Regional vulnerability assessment for debris flows in China – a CWS approach, Landslides, 13, 537–550, https://doi.org/10.1007/s10346-015-0578-1, 2016.

Dou, J., Yamagishi, H., Pourghasemi, H. R., Yunus, A. P., Xuan, S., Xu, Y., and Zhu, Z.: An integrated artificial neural network model for the landslide susceptibility assessment of Osado Island, Japan, Nat. Hazards, 78, 1749–1776, 2015.

Fall, M., Azzam, R., and Noubactep, C.: A multi-method approach to study the stability of natural slopes and landslide susceptibility mapping, Eng. Geol., 82, 241–263, 2006.

Feng, F., Wu, X., Niu, R., Xu, S., and Yu, X.: Landslide susceptibility assessment based on PSO-BP neural network, Science of Surveying Mapping, 42, 170–175, https://doi.org/10.16251/j.cnki.1009-2307.2017.10.027, 2017.

Feng, W., Zhang, T., and Zhang, Y.: Evaluating the stability of landslides in xianshizhai village and the pipeline vulnerability with their action, Journal of Geological Hazards & Environment Preservation, 25, 83–88, 2014.

Gao, C. L., Li, S. C., Wang, J., Li, L. P., and Lin, P.: The Risk Assessment of Tunnels Based on Grey Correlation and Entropy Weight Method, Geotechnical & Geological Engineering, 36, 1621, https://doi.org/10.1007/s10706-017-0415-5, 2017.

Guzzetti, F., Cardinali, M., and Reichenbach, P.: The Influence of Structural Setting and Lithology on Landslide Type and Pattern, Environ. Eng. Geosci., 2, 531–555, 1996.

Hao, J. and Liu, J.: Zonaion of Danger Degree of Geological Hazards over Lanzhou-Chengdu-Chongqing Products Pipeline, Oil & Gas Storage & Transportation, 49–53, 62, 68–69, 2008.

He, Y. and Fu, W.: Application of fuzzy support vector machine to landslide risk assessment, Journal of Natural Disasters, 18, 107–112, 2009.

Ho, K., Leroi, E., and Roberds, B.: Quantitative Risk Assessment: Application, Myths and Future Direction, ISRM International Symposium, Melbourne, 19 November 2000.

Hong, H., Pradhan, B., Xu, C., and Bui, D. T.: Spatial prediction of landslide hazard at the Yihuang area (China) using two-class kernel logistic regression, alternating decision tree and support vector machines, Catena, 133, 266–281, https://doi.org/10.1016/j.catena.2015.05.019, 2015.

Hsu, K. L., Gupta, H. V., and Sorooshian, S.: Artificial neural network modeling of the rainfall-runoff process, Water Resour. Res., 31, 2517–2530, https://doi.org/10.1029/95WR01955, 1995.

Hu, H., Dong, P., and Pan, J.: The Hail Risk Zoning in Beijing Integrated with the Result of Its Loss Assessment, Journal of Applied Meteorological Science, 22, 612–620, 2011.

Hu, W., Xu, Q., Wang, G. H., Asch, T. W. J. V., and Hicher, P. Y.: Sensitivity of the initiation of debris flow to initial soil moisture, Landslides, 12, 1139–1145, https://doi.org/10.1007/s10346-014-0529-2, 2015.

Huo, F., Wang, W., Cao, Y., Wang, F., and Bureau, C. P.: China's Construction Technology of Oil and Gas Storage and Transportation and Its Future Development Direction, Oil Forum, 35, 44–51, 2016.

Inaudi, D. and Glisic, B.: Reliability and field testing of distributed strain and temperature sensors, P. Soc. Photo.-Opt. Ins., 6167, 2586–2597, https://doi.org/10.1117/12.661088, 2006.

Jaiswal, P., Westen, C. J. V., and Jetten, V.: Quantitative landslide hazard assessment along a transportation corridor in southern India, Eng. Geol., 116, 236–250, https://doi.org/10.1016/j.enggeo.2010.09.005, 2010.

Jia, Y., Zhao, J., Nan, Z., and Zhao, C.: The Application of Entropy-right Method to the Study of Ecological Security Evaluation of Grassland – A Case Study at the Ecological Security Evaluation of Grassland to Pastoral Area of Gansu, Journal of Arid Land Resources Environmental & Engineering Geoscience, 1, 17–21, https://doi.org/10.1016/S1872-5791(08)60002-0, 2007.

Jin, Y. and Meng, J. J.: Assessment and forecast of ecological vulnerability: A review, Chinese Journal of Ecology, 30, 2646–2652, 2011.

Ke, F. and Li, Y.: The forecasting method of landslides based on improved BP neural network, Geotechnical Investigation & Surveying, 42, 55–60, 2014.

Li, B. S. and Gao, Y. J.: Application of the improved fuzzy analytic hierarchy process for landslide hazard assessment based on RS and GIS, Paper presented at the International Conference on Intelligent Earth Observing and Applications, 9 December 2015, Guilin, https://doi.org/10.1117/12.2207381, 2015.

Li, G., Zhang, P., Li, Z., Ke, Z., and Wu, G.: Safety length simulation of natural gas pipeline subjected to transverse landslide, Electronic Journal of Geotechnical Engineering, 2016 (21.12), 4387–4399, http://www.ejge.com/2016/Ppr2016.0375ma.pdf (last access: May 2017), 2016.

Li, J.: Wenchuan Earthquake and Secondary Geological Hazard Assessment Based on RS/GIS Technology, Master, China University of Geosciences, Beijing, China, 2010.

Li, J., Feng, J., Wang, W., and Zhang, F.: Spatial and Temporal Changes in Solar Radiation of Northwest China Based LM-BP Neural Network, Scientia Geographica Sinica, 36, 780–786, https://doi.org/10.13249/j.cnki.sgs.2016.05.017, 2016.

Li, P. L., Tian, W. P., and Li, J. C.: Analysis of landslide stability based on BP neural network, Journal of Guangxi University, 38, 905–911, https://doi.org/10.19406/j.cnki.cqkjxyxbzkb.2011.01.029, 2011.

Li, S.: The Risk Assessment Study on the Environmental Geological Hazards along the West-East Nature Gas Pipeline, Master thesis, SouthWest JiaoTong University, Chengdu, China, 2008.

Li, S., Jian, J., Wu, Z., Li, S., Li, H., Bai, K., Ke, Q., Xu, Y., and Hu, Y.: A Design of the Geo-Environmental Management Database System for Guangyuan, City, Journal of Geological Hazards and Environment Preservation, 23, 36–42, 2012.

Liu, P. and Zhang, X.: Research on the supplier selection of a supply chain based on entropy weight and improved ELECTRE-III method, Int. J. Prod. Res., 49, 637–646, https://doi.org/10.1080/00207540903490171, 2011.

Liu, Y.: The characteristic and evaluation of collapse and landslide disaster along du-wen highway in Wenchuan earthquake region, Master, Lanzhou University, Lanzhou, 2009.

Liu, Y., Shi, Y., Lu, Q., Xiao, H., and Wu, S.: Risk Assessment of Geological Disasters in Single Pipe Based on Scoring Index Method: A Case Study of Soil Landslide, Natural Gas Technology & Economy, 9, 57–61, 79, 2015.

Luo, Z. F. and Tan, D. J.: Landslide Hazard Evaluation in Debris Flow Catchment Area Based on GIS and Information Method, China Safety Science Journal, 21, 144–150, https://doi.org/10.1631/jzus.B1000265, 2011.

Mansour, M. F., Morgenstern, N. R., and Martin, C. D.: Expected damage from displacement of slow-moving slides, Landslides, 8, 117–131, https://doi.org/10.1007/s10346-010-0227-7, 2011.

Pal, R.: Entropy Production in Pipeline Flow of Dispersions of Water in Oil, Entropy, 16, 4648–4661, https://doi.org/10.3390/e16084648, 2014.

Peng, L., Deng, W., Zhang, H., Sun, J., and Xiong, J.: Focus on economy or ecology? A three?dimensional trade-off based on ecological carrying capacity in southwest China, Nat. Resour. Model., e12201, 2018.

Qiu, D., Niu, R., Zhao, Y., and Wu, X.: Risk Zoning of Earthquake-Induced Landslides Based on Slope Units: A Case Study on Lushan Earthquake, Journal of Jilin University, 45, 1470–1478, https://doi.org/10.13278/j.cnki.jjuese.201505201, 2015.

Rafiq, L. and Blaschke, T.: Disaster risk and vulnerability in Pakistan at a district level, Geomat. Nat. Haz. Risk., 3, 324–341, https://doi.org/10.1080/19475705.2011.626083, 2012.

Ray, P. K. C., Dimri, S., Lakhera, R. C., and Sati, S.: Fuzzy-based method for landslide hazard assessment in active seismic zone of Himalaya, Landslides, 4, 101–111, https://doi.org/10.1007/s10346-006-0068-6, 2007.

Sari, D. A. P., Innaqa, S., and Safrilah: Hazard, Vulnerability and Capacity Mapping for Landslides Risk Analysis using Geographic Information System (GIS), IOP Conference Series: Materials Science and Engineering, 209, 012106, https://doi.org/10.1088/1757-899X/209/1/012106, 2017.

Sarkar, S. and Gupta, P. K.: Techniques for Landslide Hazard Zonation – Application to Srinagar-Rudraprayag Area of Gar, J. Geol. Soc. India, 65, 217–230, 2005.

Shi, S.: Risk Analysis for Pipeline Construction about Third Party Damage Based on Triangular Fuzzy Number and Fault Tree Theory, Journal of Chongqing University of Science & Technology, 13, 91–94, https://doi.org/10.19406/j.cnki.cqkjxyxbzkb.2011.01.029, 2011.

Su, G. and Deng, F.: On the Improving Backpropagation Algorithms of the Neural Networks Based on MATLAB Language: A Review, Bulletin of Science & Technology, 2, 130–135, https://doi.org/10.13774/j.cnki.kjtb.2003.02.012, 2003.

Wang, P., Xu, Z., Bai, M., Du, Y., Mu, S., Wang, D., and Yang, Y.: Landslide Risk Assessment Expert System Along the Oil and Gas Pipeline Routes, Adv. Mat. Res., 418–420, 1553–1559, https://doi.org/10.4028/www.scientific.net/AMR.418-420.1553, 2012.

Wang, Y., Hao, J., Zhao, F., and Fang, L.: A Discussion on Regional Risk Zoning of Geological Hazard in the Worst-hit Area of the Wenchuan Earthquake in Shaanxi Province, Journal of Catastrophology, 26, 35–39, https://doi.org/10.1007/s12583-011-0163-z, 2011.

Wu, Z. and Wang, H.: Super-resolution Reconstruction of SAR Image based on Non-Local Means Denoising Combined with BP Neural Network, 2016.

Wu, T. H., Tang, W. H., and Einstein, H. H.: Landslides: investigation and mitigation, chapter 6 – landslide hazard and risk assessment, Transportation Research Board, 106–118, 1996.

Xiang, L. Z., Cui, P., Zhang, J. Q., Huang, D. C., Fang, H., and Zhou, X. J.: Triggering factors susceptibility of earthquake-induced collapses and landslides in Wenchuan County, Journal of Sichuan University, 42, 105–112, 2010.

Xin, Y., Chong, X. U., and Dai, F. C.: Contribution of strata lithology and slope gradient to landslides triggered by Wenchuan Ms 8 earthquake, Sichuan, China, Geological Bulletin of China, 28, 1156–1162, 2009.

Xiong, H., Ran, Y., Xiong, G., Li, S., and Ye, L.: Study on deformation prediction of landslide based on genetic algorithm and improved BP neural network, Kybernetes, 39, 1245–1254, 2010.

Ye, C., Jiang, H., Yao, A., Xia, Q., and Zhao, X.: Study on risk controlling method of third party construction damage on oil and gas pipeline, Journal of Safety Science & Technology, 9, 140–145, 2013.

Yun, L. and Kang, L.: Reliability Analysis of High Pressure Buried Pipeline under Landslide, Appl. Mech. Mater., 501–504, 1081–1086, https://doi.org/10.4028/www.scientific.net/AMM.501-504.1081, 2014.

Zhang, Q., Xu, Q., Wu, L., and Li, J.: BP neural network model for forecasting volume of landslide group in Nanjiang, Hydrogeology and Engineering Geology, 42, 134–139, https://doi.org/10.16030/j.cnki.issn.1000-3665.2015.01.23, 2015

Zhang, Y., Shi, J., Gan, J., and Liu, C.: Analysis of Distribution Characteristics and Influencing Factors of Secondary Geohazards in Guangyuan City – Taking Chaotian District as an Example, Journal of Catastrophology, 26, 75–79, https://doi.org/10.1007/s12182-011-0118-0, 2011.

Zheng, J. Y., Zhang, B. J., Liu, P. F., and Wu, L. L.: Failure analysis and safety evaluation of buried pipeline due to deflection of landslide process, Eng. Fail. Anal., 25, 156–168, https://doi.org/10.1016/j.engfailanal.2012.05.011, 2012.